

# A Game-Theoretic Approach for Hierarchical Policy-Making

Feiran Jia, Aditya Mate, Zun Li, Shahin Jabbari, Mithun Chakraborty  
 Milind Tambe, Michael Wellman, Yevgeniy Vorobeychik

March 1, 2025

## Abstract

We present the design and analysis of a multi-level game-theoretic model of hierarchical policy-making, inspired by policy responses to the COVID-19 pandemic. Our model captures the potentially mismatched priorities among a hierarchy of policy-makers (e.g., federal, state, and local governments) with respect to two main cost components that have opposite dependence on the policy strength, such as post-intervention infection rates and the cost of policy implementation. Our model includes a crucial third factor in decisions: a cost of non-compliance with the policy-maker immediately above in the hierarchy, such as non-compliance of state with federal policies. Our first contribution is a closed-form approximation of a recently published agent-based model to compute the number of infections for any implemented policy. Second, we present a novel equilibrium selection criterion that addresses common issues with equilibrium multiplicity in our setting. Third, we propose a hierarchical algorithm based on best response dynamics for computing an approximate equilibrium of the hierarchical policy-making game consistent with our solution concept. Finally, we present an empirical investigation of equilibrium policy strategies in this game in terms of the extent of free-riding as well as fairness in the distribution of costs, depending on parameters such as the degree of centralization and disagreements about policy priorities among the agents.

## 1 Introduction

Democratic governments and institutions typically have a hierarchical structure. For example, policies in the U.S. emerge from complex interactions among the federal and state governments, as well as county boards and city councils and mayors. Similar structure exists in Canada and in European democracies. Such policy interactions are hierarchical, with higher levels in the hierarchy able to impose some constraints on the policies immediately below (e.g., the U.S. federal government can constrain what state policies can be). Violations of these constraints, in turn, entail a non-compliance cost to the violator, such as legal costs, penalties, or reputation loss. Many examples of such hierarchical policy structure commonly arise, such as in educational and vaccination decisions, as well as in devising policies for controlling a pandemic. Take COVID-19 social distancing policies as a concrete example. These policies commonly include recommendations at the national level, guidelines and restrictions at the state/province/district level, and policies for specific counties or cities. Moreover, a common feature of such hierarchical policy-making is that what ultimately matters are the policies actually deployed at the lowest level, since these are often most practical to enforce.

In general, policies are contentious. Agents at all levels of the policy-making hierarchy may disagree about the best policies, or more fundamentally, about the particular tradeoffs made in devising policies. For example, COVID-19 social distancing measures have considerable costs, both economic and socio-psychological, but lack thereof results in more people who become infected; different institutions disagree on how to trade off these concerns.

We propose a general model of hierarchical policy-making as a game among the policy-makers at all levels of the hierarchy. In this game, policies at the higher levels have an impact by imposing non-compliance costs on lower levels, but ultimate implementation of policies happens at the lowest level. Each agent in this game trades off two types of costs: policy *implementation cost* (e.g., socio-psychological or economical

impacts of lockdowns) and *policy impact cost* (e.g., number of COVID-19 infections). Besides the impact on the structure of agent utilities, the hierarchy also impacts the sequence of moves: agents at higher levels precede lower levels (e.g. by announcing guidelines), with the latter observing and reacting to the policy recommendations by levels above them.

In our game-theoretic model, each agent’s action/pure strategy is a single, bounded scalar that represents the degree of social distancing in the pandemic-response context. Our first contribution is a novel solution concept which refines the subgame perfect Nash equilibrium, accounting for commonly occurring indifferences. Our second contribution is an analytic version of a recently proposed agent-based model (ABM) for COVID-19 pandemic spread estimation that accounts for social distancing [28]; we show that our analytic model closely mirrors short-term behavior of the ABM with a much shorter computational cost compared to the ABM.

We use our modeling framework to experimentally investigate possible phenomena arising from decentralized policy-making.

One of our questions relates to *policy free-riding*: Is it possible that (in equilibrium) a player lower in the hierarchy adopts a weak policy with a low implementation cost while imposing a negative externality on another player (perhaps on the same level) and hence also enjoying lower infection numbers owing to the latter player’s stronger policy? Can a higher-level policy-maker mitigate such free-riding via non-compliance penalties? We show that the answer depends in a complex manner on different parameters such as initial infection rates, degree of contact among different parts of the population, weights on different types of cost, and the non-compliance cost structure. Our second set of experiments measures the *fairness* in the distribution of costs as a function of model parameters as well as degrees of centralization.

## 1.1 Related work

Our work is related to the line of research applying the social and behavioral sciences to the cost-benefit analysis of both centralized and decentralized decision-making under pandemic/epidemic conditions [24]. Some papers approach these trade-offs from an *optimal control* perspective [5, 17–19]. Others study the equilibria of various game-theoretic models of *individuals* deciding whether to follow guidelines for preventive measures (distancing, vaccination, etc.) and treatment, possibly against the (perceived) aggregate behavior of the population, under various models of disease propagation; e.g. the differential game model [15], the “wait and see” model of vaccinating behavior [1], evolutionary game-theoretic models [2, 10], and various others [3, 4, 8, 22] (see, e.g. [23] for a summary). We distinguish from these works by modeling the strategic interactions among *ideologically diverse, hierarchical policymakers* with explicit *non-compliance penalties*, and experimentally assess the impact of such interactions upon the actually implemented policies under various parameter settings.

Also related is the literature on ABM for pandemic spread and response policies that account for preferences/incentives of individuals [6, 9, 28]. [28] is of particular importance since our policy impact cost is computed by a closed-form approximation to their model. Other recent work includes the assessment of the impact of prevention and containment policies on the spread COVID-19 via causal analysis [12], Gaussian processes [14], and state-of-the-art data-driven non-pharmaceutical intervention models [20].

Instead of an analytic treatment, we empirically compute the (approximate) equilibrium of our complex, multi-level, continuous-action game using algorithmic approaches that exploit the structure of the problem. Thus, our methods belong to the category of *empirical game-theoretic analysis* (see, e.g. [7, 25–27]).

# 2 A Model of Hierarchical Policy-Making

## 2.1 The Game Model

Consider as a running example COVID-19 hierarchical policy-making with three levels of decision-makers: Government (a single agent), States, and Counties. Each agent is a player in a game and chooses a social distancing policy (recommended or enforced). Next, we present a formal game theoretic model of this kind

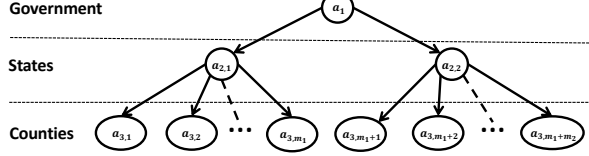


Figure 1: Hierarchy of policy-makers with 3 levels: Government, States and Counties.

of hierarchical policy-making, focusing on strategic interactions among players both within and across the levels in this hierarchy.

Let  $[m]$  denote the set  $\{1, 2, \dots, m\}$  for any  $m \in \mathbb{Z}^+$ . We represent the *players* in the *hierarchical policy-making game (HPMG)* by *nodes* in a directed rooted tree (we will use the terms players and nodes interchangeably), as illustrated in Figure 1 for our running example. A general *HPMG* has  $L > 1$  levels or layers. Each level  $l \in [L]$  is associated with a set of nodes/players, denoted by  $\mathcal{L}_l$ , with  $n_l = |\mathcal{L}_l|$  the number of players in level  $l$ . Without loss of generality, let  $n_1 = 1$  (we can always add a dummy layer with a single player who has a single strategy); we call the player in level 1, denoted by  $a_1$  the *root-node*. The  $i^{\text{th}}$  node/player in an arbitrary level  $l$  is denoted by  $a_{l,i}$ . For each player in each level  $l < L$ ,  $a \in \mathcal{L}_l$ , let  $\chi(a)$  be the set of its children in the tree; clearly,  $|\chi(a)| \geq 0$  for every  $a$ , and  $\sum_{a \in \mathcal{L}_l} |\chi(a)| = n_{l+1}$  for each  $l$ . Likewise, for every player  $a \in \mathcal{L}_l$  and for each  $l > 1$ , let  $\pi(a)$  be its unique parent in the tree, where a directed edge goes from a parent to its child. In our running example in Figure 1,  $a_1$  is the Government in level 1, level 2 consists of two States, both children of  $a_1$ ,  $\chi(a_1) = \{a_{2,1}, a_{2,2}\}$ , and level 3 consists of Counties.

Each player  $a$  can take a scalar *action*  $\alpha_a \in [0, 1]$ .  $\bar{\alpha}$  denotes the profile of actions of all players, and  $\bar{\alpha}_l$  the restriction of this profile to a particular level  $l$ . In our pandemic-response policy-making example,  $\alpha_a$  is an abstraction of the policy adopted by  $a$ , capturing the *the extent of overall activity* (conversely,  $1 - \alpha_a$  represents the extent of social distancing implemented/recommended by  $a$ ). Thus, small  $\alpha_a$  corresponds to the greatest reduction in infection spread (due to stricter social distancing). On the other hand, a large  $\alpha_a$  will entail a higher policy implementation cost, such as socio-economic and psychological costs of social distancing. At the extremes of our illustration,  $\alpha_a = 1$  signifies no intervention, while  $\alpha_a = 0$  corresponds to a complete lockdown.

*HPMG* is a sequential game in which players make strategic decisions following the sequence of layers. Specifically, the player in level 1 moves (i.e., chooses a strategy) first, followed by all players in level 2, who first observe the strategy of  $a_1$  and simultaneously choose a joint strategy profile in response. This is then followed by all players in level 3, and so on. Thus, all players in the same level  $l$  make strategic choices simultaneously.

Because all the utilities in our main application of this model (COVID-19 social distancing policies) are negative (i.e., costs), we next define the general model in terms of costs (negative utilities). The cost function of each player  $a$  has three components: *policy impact cost*,  $C_a^{\text{inc}}(\bar{\alpha})$ , *policy implementation cost*,  $C_a^{\text{dec}}(\bar{\alpha})$ , and, for each player in levels  $l > 1$ , *non-compliance cost*,  $C_a^{\text{NC}}(\alpha_a, \alpha_{\pi(a)})$ . In the COVID-19 example, policy impact cost is a measure of infection spread (number of people infected in the player's geographic area, say), while implementation cost can be a psychological and economic costs of a lockdown. The non-compliance cost, in turn, is a penalty imposed by a policy-maker upon an agent within its jurisdiction for deviating from its recommendation (e.g., a fine, litigation costs, or reputational harm). An important piece of structure to the policy implementation and impact costs is that they directly depend for a player  $a$  not on the full profile of strategies by all players, but only on the layer  $l$  of the player  $a$  if  $l = L$ , and only the layer immediately below otherwise. To formalize, we introduce for each player  $a$  the notion of its *share*  $\mu_a \in [0, 1]$ . In our running example, a node's share can be interpreted as the proportion of the total population of the country that is under the jurisdiction of the corresponding player (e.g., the share of a state is the proportion of the total population that resides in this state). Thus,  $\mu(a_1) = 1$ , while the shares of the nodes in the lowest level  $L$  are arbitrary, except for the constraint  $\sum_{a \in \mathcal{L}_L} \mu_a = 1$ . For a level  $1 < l < L$ , we have  $\mu_a = \sum_{a' \in \chi(a)} \mu_{a'}$  for every  $a \in \mathcal{L}_l$ . We now use the notion of shares to formally define the impact and implementation costs of

policies.

- For each lowest-level player  $a \in \mathcal{L}_L$ ,  $C_a^{\text{inc}}(\bar{\alpha})$  depends only on  $\bar{\alpha}_L$ , lies in  $[0, 1]$ , and is non-decreasing in each  $\alpha_a \in \bar{\alpha}_L$ ; we provide further specifics of this function for our pandemic-response example in Section 2.3. For a higher-level player  $a \in \mathcal{L}_l$ ,  $l < L$ , this cost is the share-weighted aggregate of those of its child-nodes:

$$C_a^{\text{inc}}(\bar{\alpha}) = \frac{1}{\mu_a} \sum_{a' \in \chi(a)} \mu_{a'} C_{a'}^{\text{inc}}(\bar{\alpha}).$$

- For each  $a \in \mathcal{L}_L$ ,  $C_a^{\text{dec}}(\bar{\alpha}) \in [0, 1]$  depends only on, and is non-increasing, in  $\alpha_a$ ; in particular, in our pandemic-response example, we simply focus on the function  $C_a^{\text{dec}}(\bar{\alpha}) = 1 - \alpha_a$ . Also, for each  $a \in \mathcal{L}_l$ ,  $l < L$ ,

$$C_a^{\text{dec}}(\bar{\alpha}) = \frac{1}{\mu_a} \sum_{a' \in \chi(a)} \mu_{a'} C_{a'}^{\text{dec}}(\bar{\alpha}).$$

Finally, we consider two variants of the non-compliance cost: *one-sided* under which there is no penalty for an  $\alpha$  lower than that of the parent (capturing scenarios such as a policy-maker only punishing policy responses weaker than its recommendation), and *two-sided* under which any deviation is penalized regardless of direction [16], with the discrepancy being measured by the Euclidean distance for either variant:

$$C_a^{\text{NC}}(\alpha, \alpha') = \begin{cases} (\max\{0, \alpha - \alpha'\})^2, & \text{if one-sided;} \\ (\alpha - \alpha')^2, & \text{if two-sided.} \end{cases}$$

Finally, each player  $a \in \mathcal{L}_l$  for  $l > 1$  has an idiosyncratic set of *weights*  $\kappa_a \geq 0$  and  $\eta_a \geq 0$  that trade its three cost components off against each other via a convex combination, and account for differences in ideology. Thus, the overall cost of such a player  $a$  is given by

$$C_a(\bar{\alpha}) := \kappa_a C_a^{\text{inc}}(\bar{\alpha}) + \eta_a C_a^{\text{dec}}(\bar{\alpha}) + \gamma_a C_a^{\text{NC}}(\alpha_a, \alpha_{\pi(a)}),$$

where  $\gamma_a = 1 - \kappa_a - \eta_a$ . The player  $a_1$  obviously has no non-compliance issues, hence it has only one weight  $\kappa_{a_1} > 0$ , its overall cost being

$$C_{a_1}(\bar{\alpha}) := \kappa_{a_1} C_{a_1}^{\text{inc}}(\bar{\alpha}) + (1 - \kappa_{a_1}) C_{a_1}^{\text{dec}}(\bar{\alpha}).$$

## 2.2 Solution Concept

The solution concept we are primarily interested in is a *pure-strategy subgame perfect Nash equilibrium* (PSPNE) [21] of our continuous-action game which is sequential-move between levels and simultaneous-move within a level. However, the game may have multiple such equilibria, leading to an *equilibrium selection problem*.

An extreme but simple motivating scenario which gives rise to a multiplicity of equilibria, many of which are unreasonable, is when a lowest-level player  $a$  has non-compliance weight  $\gamma_a = 1$  under a one-sided cost structure: player  $a$  would be indifferent among all values  $\alpha_a \in [0, \alpha_{\pi(a)}]$  since any such value induces an overall cost of 0. Such indifference could also characterize the best response of a higher-level player. Consider a two-level variant of the game in Figure 1 (e.g., when counties are constrained to be compliant with the respective states); for each state  $a \in \{a_{2,1}, a_{2,2}\}$ , let  $\kappa_a = 0$  and  $\eta_a = 0.6$ , hence  $\gamma_a = 0.4$ . Straightforward calculations show that the local minimum  $\alpha_a^*$  of the overall cost of any such state  $a$  over  $[0, \alpha_{a_1}]$  is  $\alpha_a^* = \alpha_{a_1}$  with a cost of  $0.6(1 - \alpha_{a_1})$  and that over  $(\alpha_{a_1}, 1]$  is

$$\alpha_{a'}^* = \begin{cases} 1, & \text{cost} = 0.4(1 - \alpha_{a_1})^2, \quad \alpha_a \geq 0.25; \\ \alpha_{a_1} + 0.75, & \text{cost} = 0.375 - 0.6\alpha_{a_1}, \quad \text{otherwise.} \end{cases}$$

Thus, the unique best response of either state (whose costs are independent of each other) to *any* government policy  $\alpha_{a_1} \geq 0.25$  is 1, i.e., there are infinitely many equilibria with the government recommending any  $\alpha_{a_1} \geq 0.25$  but each state choosing 1 regardless. The fact that the government would recommend a policy

intervention (which could be as strong as  $\alpha_{a_1} = 0.25$ ) knowing fully well that both states would choose no intervention even under the threat of a non-compliance penalty seems absurd, but this absurdity cannot be eliminated by the above solution concept.

With this in mind, we propose and use the following equilibrium selection criterion. For any player  $a \in \mathcal{L}_l$ ,  $l < L$ , define its *social cost*  $\text{SC}_a(\bar{\alpha}_{\chi(a)})$  for any action profile  $\bar{\alpha}_{\chi(a)}$  of its children as the share-weighted aggregate of the overall costs of its children, that is:  $\text{SC}_a(\bar{\alpha}_{\chi(a)}) := \frac{1}{\mu_a} \sum_{a' \in \chi(a)} \mu_{a'} \mathbf{C}_a(\bar{\alpha})$ . Evidently, this quantity is, in general, distinct from  $\mathbf{C}_a(\bar{\alpha})$ .

If multiple values of  $\alpha_a$  induce equilibria for a particular  $\bar{\alpha}_{\chi(a)}$ , then we will pick the  $\alpha_a$  which minimizes  $\text{SC}_a(\bar{\alpha}_{\chi(a)})$ , breaking further ties in favor of a higher  $\alpha_a$  (i.e., smaller policy impact). We refer to this solution concept, which is a refinement of PSPNE, as *minimal-impact pure-strategy subgame perfect Nash equilibrium (MI-PSPNE)*.

In general, a MI-PSPNE will not exist. Consequently, we will seek to compute an  $\epsilon$ -MI-PSPNE, where  $\epsilon$  is the highest benefit from deviation by any player  $a$ . Below (Section 3) we present a general approach for finding such approximate equilibria in our setting.

## 2.3 Infection Dynamics and Cost

We now come to the particular instantiation of  $\mathbf{C}_a^{\text{inc}}(\cdot)$  for each of the lowest-level players  $a \in \mathcal{L}_L$  (Counties in Figure 1). Recently, Wilder et al. [28] developed and analyzed an agent-based model (ABM) for COVID-19 spread that accounts for the *degree of contact* (both within and between households) among individuals from different parts of a population.<sup>1</sup> However, this ABM is computationally expensive, making its use for equilibrium computation impractical at scale. In this section, we will derive a closed-form model of infection spread that (as we show below) relatively closely mirrors the expected number of infections of the ABM over a short horizon.

Let  $N_a$  and  $I_a^0$  denote the fixed population of County  $a$  and the number of infections in  $a$  before policy intervention respectively. An individual who is not currently infected but can develop an infection on contact with someone infected is *susceptible*. We call an individual from County  $a'$  *active* in County  $a$  if that individual is capable of making contact (through travel etc.) with a susceptible individual in County  $a$ ; if  $a' = a$ , we say that the individual is active within County  $a$ . A major parameter of the ABM is the *transport matrix*  $R = \{r_{aa'}\}_{a,a' \in \mathcal{L}_L}$ , where  $r_{aa'} \geq 0$  is the proportion of the population of County  $a'$  that is active in County  $a$  in the absence of an intervention. Thus, in the absence of policy intervention, the total number of individuals from County  $a'$  active in County  $a \neq a'$  is  $N_{a'} r_{aa'}$  and the total number of infected individuals from County  $a'$  active in County  $a \neq a'$  is  $I_{a'}^0 r_{aa'}$ .

The policy  $\alpha_a$  affects the population in two ways: it scales down both the susceptible and active sub-populations. In other words, under the policy intervention, County  $a$  has  $(N_a - I_a^0)\alpha_a$  susceptible individuals, and there are  $N_{a'}\alpha_{a'}r_{aa'}$  active individuals in County  $a$  from County  $a'$ , out of whom  $I_{a'}^0\alpha_{a'}r_{aa'}$  are (initially) infected. Hence, the proportion of infected active individuals in County  $a$  is given by

$$\rho_a(\bar{\alpha}_L) := \frac{\sum_{a' \in \mathcal{L}_L} I_{a'}^0 \alpha_{a'} r_{aa'}}{\sum_{a' \in \mathcal{L}_L} N_{a'} \alpha_{a'} r_{aa'}}.$$

We will now focus on an arbitrary susceptible individual in County  $a$  and lay down our assumptions on the process why which she may contract an infection: This individual makes actual contact with a random sample of  $X$  active individuals drawn from a Poisson distribution with mean  $C$ , which is a parameter in our model [28]; this distribution is fixed across all individuals in all Counties, and all these contacts are mutually independent. The next assumption is that, in this sample of  $X$  contacts for a susceptible individual in County  $a$ , the proportion of infected individuals is  $\rho_a(\bar{\alpha}_L)$ .

Let  $p \in (0, 1)$  denote the probability that a susceptible individual becomes infected upon contact with an infected individual, i.e. the probability that contact with an infected individual does not infect a susceptible individual is  $(1 - p)$ . Since all  $X\rho_a(\bar{\alpha})$  infected contacts of an arbitrary susceptible individual are mutually

---

<sup>1</sup>The model in Wilder et al. [28] is an individual-level variant of the well-known susceptible-exposed-infectious-recovered or SEIR model but this paper assumes that every exposed person eventually becomes infected after an incubation period.

independent, the probability that the susceptible individual develops an infection is  $1 - (1 - p)^{X \rho_a(\bar{\alpha})}$ . We also interpret this as the proportion of the  $(N_a - I_a^0)\alpha_a$  susceptible individuals in County  $a$  who end up getting infected. Let  $\text{Infect}_a(\bar{\alpha})$  denote the *expected number of additional, post-intervention infections* in County  $a$ . Thus,

$$\text{Infect}_a(\bar{\alpha}) = \mathbb{E}_X[(N_a - I_a^0)\alpha_a(1 - (1 - p)^{X \rho_a(\bar{\alpha})})] = (N_a - I_a^0)\alpha_a(1 - \mathbb{E}_X[((1 - p)^{\rho_a(\bar{\alpha})})^X]).$$

Define  $y_a(\bar{\alpha}_L) := (1 - p)^{\rho_a(\bar{\alpha})}$ . Since  $X \sim \text{POISSON}(C)$ , Proposition 1 in Appendix A tells us that

$$\text{Infect}_a(\bar{\alpha}) = (N_a - I_a^0)\alpha_a(1 - e^{-C(1 - y_a(\bar{\alpha}_L))}). \quad (1)$$

Finally, we define the infection cost to be  $C_a^{\text{inc}}(\bar{\alpha}) = \text{Infect}_a(\bar{\alpha})/N_a$ .

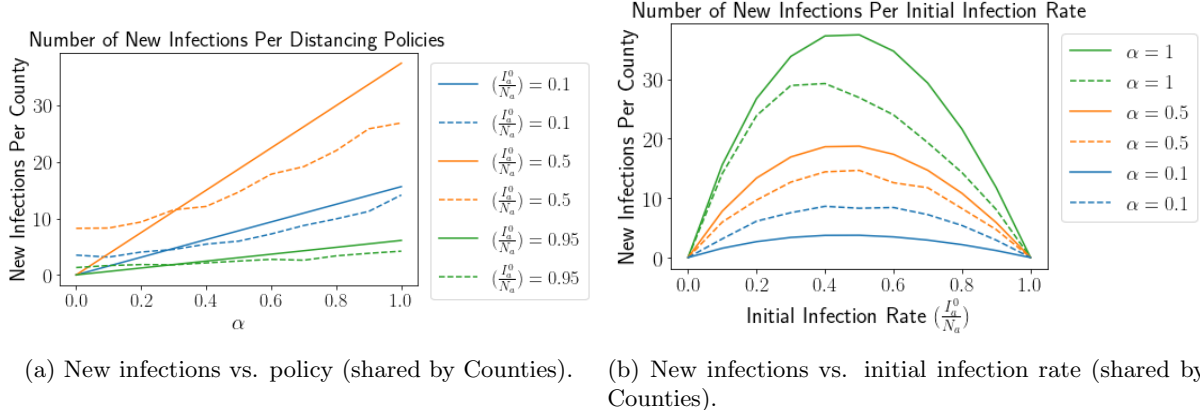


Figure 2: Comparison of ABM output (solid lines) with closed-form approximation (dashed lines).

We ran some preliminary experiments comparing Equation (1) with the actual output of the ABM [28]; partial results are shown in Figure 2. Note that Equation (1) is a one-shot formula, whereas the ABM computes contacts and infections recursively over several time-periods with an initial *incubation period* so that the effect of the first-period contacts are manifested only after a delay. Hence, we contrast the ABM output after 8 periods (to account for the average incubation period of 7 days [11]) with the above closed-form estimation. In the experiments we report, we have 2 States under the Government, each State having 2 Counties (4 Counties in total); each County  $a$  has a population of  $N_a = 250$ ; the transport matrix is symmetric, given by  $r_{aa'} = 0.25$  for every pair of Counties  $a, a'$ . We set  $p = 0.047$  [28] and  $C = 15$  (calculated based on Prem et al. [13]). For each set of experiments (represented by a separate color in Figure 2), each County has the same *initial infection rate*  $I_a^0/N_a$  and applies the same policy  $\alpha$ . In Figure 2a, we vary  $\alpha$  on the x-axis, for different (fixed) values of  $I_a^0/N_a$  which is the same for all Counties; similarly, in Figure 2b, for different policies, we vary the initial infection rates. The plots indicate qualitative similarity between the ABM and our approximation; a salient point of similarity is that the additional number of infections decreases as the initial infection rate gets higher or lower than a middling point, everything else remaining the same. This is because a higher infection rate implies less “room for growth” due to a fixed population, whereas a lower value of the same rate causes fewer further infections over the same horizon.

### 3 Solution Approach

Our HPMG model is essentially an extensive-form game model endowed with one-dimensional action space for each agent resulting in a non-convex strategic landscape. To seek for PSPNE in the hierarchical game(HG), we propose a backward induction algorithm incorporated with a payoff point query interface and a best response computation component solving for a joint-policy profile in equilibrium. The algorithm exploits

---

**ALGORITHM 1: HG-PSPNE**


---

**Input:**  $\alpha_{1:l-1}$ .  
**Parameter:**  $\text{param}_l = \{\mathbf{T}_{l:L}, \mathbf{k}_{l:L}, \mathbf{e}_{l:L}\}$ .  
1: Let  $t \leftarrow 1, \epsilon_l \leftarrow \infty$ . Initialize  $\bar{\alpha}_l$  randomly.  
2: **while**  $t \leq T_l$  or  $\epsilon_l \leq e_l$  **do**  
3:   **for**  $a_{l,i}$  in  $\mathcal{L}_l$  **do**  
4:     **if**  $l$  is the lowest level  $L$  **then**  
5:        $\alpha'_{a_{l,i}} \leftarrow \arg \min_{\alpha_{l,i}} \mathbf{C}_{a_{l,i}}(\bar{\alpha})$   
6:     **else**  
7:        $\alpha'_{a_{l,i}} \leftarrow \arg \min_{\alpha_{l,i}} \mathbf{C}_{a_{l,i}}(\text{HG-PSPNE}(\alpha_{1:l}))$   
8:     **end if**  
9:   **end for**  
10:   Calculate  $\epsilon_l$  for profile  $\bar{\alpha}_l$  and update  $\epsilon_l$  if lower than the current value.  
11:   Pick  $k_l$  agents to best respond to  $\alpha'_{l,i}$ .  
12:    $t \leftarrow t + 1$ .  
13: **end while**  
14: **return**  $\bar{\alpha}^*$  where  $\bar{\alpha}_l^*$  has the lowest  $\epsilon_l$ .

---

the hierarchical structure by propagating strategic information between consecutive levels, detailed as follows. Given a joint action profile at levels  $1, \dots, l-1$ , the players at level  $l$  compose a simultaneous-move game whose payoffs emerge from the strategic interactions from levels below them. To obtain payoffs for a certain action profile at level  $l$ , we recursively call to the next level  $l+1$  till we reach the bottom level  $L$ . Then at level  $l$ , we use these payoffs to solve for an approximate Nash equilibrium. Since every such simultaneous-move game lacks the tractable analytic payoff structure for gradient-based optimization, in our current implementation we discretize the infinite strategy space and adopt *best response dynamics* (BRD) for equilibrium computation.

Algorithm 1 computes the  $\epsilon$ -equilibrium among players at a single level  $l$  given tunable parameters. An  $\epsilon$ -equilibrium at level  $l$  is an action profile  $\bar{\alpha}_l$  where no agent  $\alpha_{a_{l,i}}$  can decrease their cost by more than  $\epsilon$  by a unilateral deviation (Lines 3–6). Let  $\alpha_{l_1:l_2}$  denote the sequence of actions  $\bar{\alpha}_{l_1}, \dots, \bar{\alpha}_{l_2}$ ;  $\mathbf{T}_{l:L} = T_l, \dots, T_L$  the maximum numbers of steps of BRD at each level  $l > 1$ ;  $\mathbf{e}_{l:L} = e_l, \dots, e_L$  the limits of  $\epsilon$  for each level. At each round  $t < T$ , we randomly select a subset of  $k_l$  out of  $n_l$  agents to best respond simultaneously to the existing profile; we call the variant with  $k_l = n_l$  *synchronous BRD*. We report some experimental results on the dependence of the number of BRD steps to reach equilibrium on the sample size  $k_l$  in Appendix B. To increase efficiency, we should pick a subset of agents that can improve their payoffs after best-responding (Line 7). The synchronous BRD might get trapped in a cycle of moves. The way we solve this issue is to keep a memory of the moves, then check whether the new profile already exists in the memory and, if yes (i.e. a cycle is detected), we jump to a new profile and resume the BRD. Finally, the algorithm returns the profile with the lowest  $\epsilon_l$  when the termination condition is met.

To search for the best strategy, we discretize the continuous strategy space and use grid search with tie-breaking (smaller policy impact) to recover the optimum value. However, in the experiments shown Figure 2a, we observe that our approximation of the infection cost is nearly linear. Although we have no guarantees, it is reasonable to ask whether the overall cost of a lowest-level player is almost convex in its policy (given the particular closed forms we use for the implementation and non-compliance costs) and hence whether we could use *binary search* (i.e. the bisection methods) to speed up our BRD. Figure 3 shows the run-time of a two-level game for  $n_2 = 10$  to 100 players in the second level when we replace the grid search in the lowest level with the binary search under a symmetric setting (i.e. equal populations and symmetric transport matrix in level 2). In those experiments, we all find the PSPNEs with  $\epsilon_2 = 0$ . Binary search yields same results as grid search, but is more efficient.

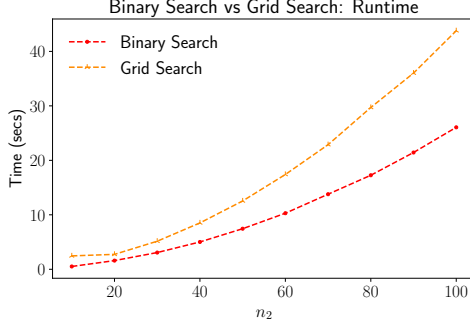


Figure 3: Run-time in secs (y-axis) of binary search and grid search as a function of  $n_2$  (x-axis) in a symmetric setting.

## 4 Experiments

In this section, we describe two sets of experiments on our HPMG framework using the methodology discussed in Section 3. Given the large and complex set of game parameters, we report the most insightful experimental results we obtained, deferring additional results to the full version. In Section 4.1, we quantify the notion of *free-riding* and explore conditions under which free-riding appears in equilibrium and can be circumvented by non-compliance penalties. In Section 4.2, we study how different degrees of centralization and mismatched priorities of players in HPMG can impact fairness in the distribution of costs. In all our experiments, we use the 3-level HPMG of Figure 1 with 2 States, denoted simply by 1 and 2 (also in subscripts), and a number of Counties (to be specified) with equal population. Moreover, we say that a setting has *transport symmetry* if the transport matrix  $R$  is proportional to an identity matrix i.e.  $r_{aa'} = 1/n_L$  for any two lowest-level players  $a, a'$ . There are infinite ways in which  $R$  could be asymmetric; we focus on a particular type of asymmetry where one subset of Counties (or more generally lowest-level players)  $\mathcal{F}$  are *globally favorite destinations* (and equally popular) and all others are equally (un)popular, i.e. for each County  $j$ ,  $r_{ij} = r^H > r^L = r_{kj}$  for each  $i \in \mathcal{F}$  and each  $k \in \mathcal{L}_3 \setminus \mathcal{F}$  for some  $0 < r^L < r^H < 1$ , and  $\sum_{i \in \mathcal{L}_3} r_{ij} = 1$ .

### 4.1 Free-riding

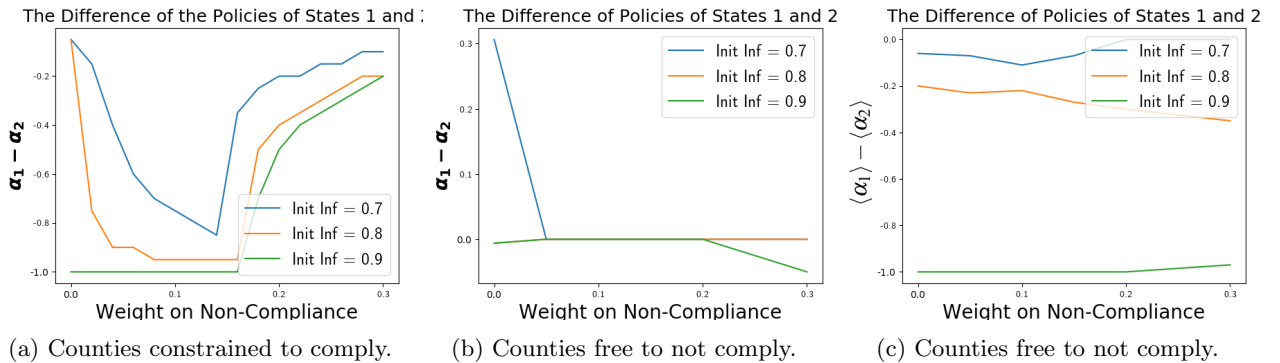


Figure 4: Free-riding (y-axis) as a function of non-compliance cost weight (x-axis). Each curve corresponds to a different initial infection rate of State 2 (Init Inf) as indicated in the legend.

We begin with the rationale for our measurement and visualization of free-riding. Suppose State 2 has

a higher initial infection (than State 1); then, intuitively, it may prefer a weak distancing policy ( $\alpha_2 \gg 0$ ) to reduce its implementation cost as most of its population is already infected; at the same time, since infection can spread from State 2, State 1 could still suffer a large infection cost unless it employs a strong distancing policy ( $\alpha_2 \ll 1$ ). This creates the possibility for State 2 to free-ride off State 1; but, whether this actually happens depends on the combination of parameters (including non-compliance issues with the Government above and Counties below) and the same possibility may be created by other conditions. We use this difference between policy strengths of the States as an indicator of the degree of free-riding. Intuitively as  $\alpha_1 - \alpha_2$  approaches  $-1$  ( $1$ ), the degree of free-riding of State 2 ( $1$ ) off State 1 ( $2$ ) increases.

In our reported experiments, we assume Government indifference between infection and implementation (i.e.  $\kappa_{a_1} = 0.5$ ) and an even split of the population between States (i.e.  $N_1 = N_2 = 500$ , hence  $\mu_1 = \mu_2 = 0.5$ ); both States use the same weight vector which we vary. The crucial difference between States is in the initial infection rate  $I_a^0/N_a$  (as we discuss shortly).<sup>2</sup> In all experiments, each State consists of 5 Counties.

Figure 4 depicts our results under transport symmetry and other conditions which we will now detail. First, we assume that all Counties are constrained to comply with their respective States so that the policies set by States 1 and 2 actually get implemented in their respective jurisdictions (i.e. we essentially have a 2-level HPMG, hence the number and weights of Counties are immaterial). In Figure 4a, we plot the variation in this policy-difference against the States' shared non-compliance weight  $\gamma_a$  under the following conditions: State 1's initial infection rate is fixed at 0.1 (low) while that of State 2 varies over  $\{0.7, 0.8, 0.9\}$ ; for either State  $a \in \{1, 2\}$ , we have  $\kappa_a = 0.9(1 - \gamma_a)$  and  $\eta_a = 0.1(1 - \gamma_a)$  for each value of the non-compliance weight. We observe that free-riding is exacerbated as State 2's initial infection rate becomes larger, although a high enough non-compliance weight will mitigate the problem. However, interestingly, lower values of the non-compliance weight also exhibit a lower degree of free-riding. Increasing the non-compliance weight forces both States to monotonically weaken their policies (towards 1) but State 1 is more conservative, maintaining a strict policy (at 0) up to a non-compliance weight of (at least) 0.15 and only then weakening its policy to the level of State 2, as shown in Figures 8 and 9 in Appendix C. This accounts for the non-monotonic dependence of free-riding on non-compliance cost weight as observed in Figure 4a.

What happens when we allow Counties to not comply with the respective States? We report results for a setting where each County's initial infection rate and weight vector is identical to that of its corresponding State. Recall that, with Counties no longer constrained to comply, State policies are *recommendations* policies whereas those that are implemented are County actions. With this mind, we report in Figures 4b and 4c the difference in State policies  $\alpha_1 - \alpha_2$  as well as the difference  $\langle \alpha_1 \rangle - \langle \alpha_2 \rangle$ , where  $\langle \alpha_a \rangle$  is the average of the equilibrium policies set by all Counties in State  $a \in \{1, 2\}$ , over the same combinations of weights and initial infection rates as Figure 4a. We find virtually no evidence of free-riding from either measure (in the extreme case represented by the lowest curve Figure 4c is perhaps better interpreted as State 2 giving up on policy intervention rather than free-riding off State 1). This indicates that distributing autonomous policy-making among several smaller-scale actors may also have a mitigating effect on free-riding, making the impact on free-riding of non-compliance penalties from the highest level weaker.

We now repeat these experiments but in a specific setting violating transport symmetry with Counties constrained to comply: we make State 1 the favorite destination with  $r^H = 0.8$  (equivalently, all Counties in State 1 are equally favored as destinations). Figure 5 shows results when the States' infection weights are  $\kappa_1 = 0.8(1 - \gamma_1)$  and  $\kappa_2 = 0.9(1 - \gamma_2)$  respectively (still with  $\gamma_1 = \gamma_2$ ), State 1's initial infection rate is fixed at 0.5 (moderate) while that of State 2 varies in  $\{0.1, 0.5, 0.6, 0.7, 0.8, 0.9\}$ , and Counties are constrained to comply. While it is true that the States' aversion to non-compliance is able to lessen free-riding monotonically and more readily as State 2's initial infection rate grows, the most salient feature is the sudden reversal in the status of the apparent free-rider as State 2's initial infection rate crosses a (high) threshold. Further inspection reveals that, although State 1 has a higher proportion of active individuals even from State 2 and cares about infections only slightly less than State 2 (but still with  $\kappa$  as high as 0.8), the initial infection rate of 0.5 is high enough for it to respond weakly ( $\alpha_1 \approx 1$ ) while State 2 weakens its policy more gradually with increase in the non-compliance weight  $\gamma_a$ , enabling State 1 to free-ride. However, once State 2's initial

<sup>2</sup>We only report results for two-sided compliance costs at all levels; we did not observe any evidence of free-riding mitigation using the one-sided variant in our experiments.

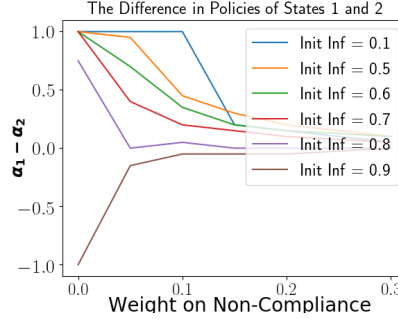


Figure 5: Free-riding (y-axis) as a function of non-compliance cost weight (x-axis). Each curve corresponds to a different initial infection rate of State 2 (Init Inf) as indicated in the legend.

infection rate becomes sufficiently high, it gives up on distancing policy even for low  $\gamma_a$ , forcing State 1 to strengthen its policy — this is reflected in the sign reversal and increased magnitude of the policy difference (Figures 10, 11, and 12 in Appendix C).

## 4.2 Fairness

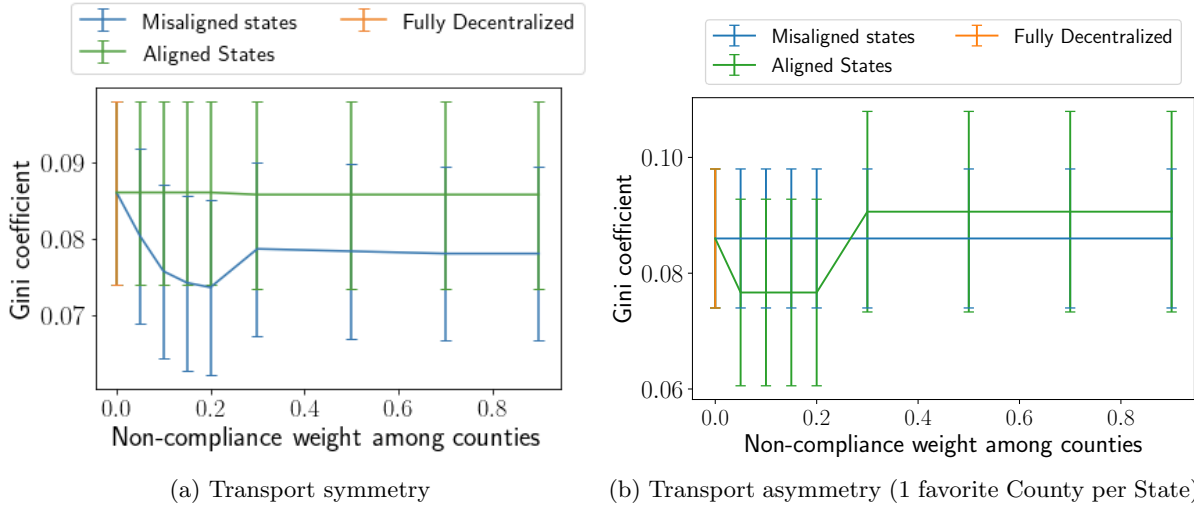


Figure 6: Gini coefficient of costs averaged over (a) 50 trials for each scenario; (b) 30 trials for *Aligned States*, 50 for each other scenario. Error bars show one standard error.

Another property of the equilibria of an HPMG worth studying is how *fair* the distribution of costs is among the Counties for different degrees of centralization and different priorities of the States. Of the many fairness concepts that exist in the literature, we apply the popular measure, the Gini coefficient, to Counties' overall costs at profile  $\bar{\alpha}$  returned by Algorithm 1:

$$\text{Gini}(\bar{\alpha}) = \frac{\sum_{a \in \mathcal{L}_3} \sum_{a' \in \mathcal{L}_3} |\mathbf{C}_a(\bar{\alpha}) - \mathbf{C}_{a'}(\bar{\alpha})|}{2n_L \sum_{a \in \mathcal{L}_3} \mathbf{C}_a(\bar{\alpha})}.$$

We report experiments with 5 Counties under each of 2 States. For the Government,  $\kappa_{a_1} = \eta_{a_1} = 0.5$ ; for each State  $b \in \{1, 2\}$ ,  $\gamma_b = 0.5$ , and there are two different scenarios of the *full game* based on the ratios

$\kappa_b/\eta_b$ : (1) *Misaligned States* if this ratio is 20/80 for State 1 and 80/20 for State 2, (2) *Aligned States* if it is 50/50 for either state. A third scenario we study is *full decentralization* where we set each County's non-compliance weight to 0 so that HPMG degenerates into a simultaneous-move game among Counties. For each scenario, we apply two treatments with respect to the transport matrix: transport symmetry and a specific asymmetry where each State has 1 County that is (universally) favorite with  $r^H = 0.35$ . In each situation, we vary the shared non-compliance weight  $\gamma_a$  of every County  $a$  as an independent variable (unless it is fixed at 0), draw a uniform random sample  $\kappa'_a \sim \mathbb{U}[0, 1]$ , and set the infection weight at  $\kappa_a = \kappa'_a(1 - \gamma_a)$ . Each set of draws for all Counties constitutes one trial. Figure 6 provide Gini coefficient scatter plots for transport symmetry and our specific asymmetry respectively. The distribution of overall costs seems reasonably and comparably fair (lower is better) across scenarios. See Appendix D for further details.

## 5 Discussion and Future Work

We have initiated the study of a new game-theoretic model motivated by decentralized, strategic policy-making under pandemic conditions, and experimentally uncovered interesting aspects of its equilibria. There are several immediate directions for future work: more extensive experimentation for other parameter configurations, including the formulation and testing of (causal) hypotheses; using the actual ABM [28] instead of our closed-form infection estimation and handling the resulting computational efficiency issues; considering more complex policies (e.g. temporally evolving strategies) and invoking more sophisticated EGTA approaches. It would also be interesting to apply HPMG or its natural variants to other problems of hierarchical decision-making within, say, a corporate or ideological (e.g. political) organization, where “superiors” can impose a non-compliance penalty or offer a compliance bonus.

## References

- [1] Samit Bhattacharyya and Chris Bauch. “Wait and see” vaccinating behaviour during a pandemic: A game theoretic analysis. *Vaccine*, 29(33):5519–5525, 2011.
- [2] Martin Brüne and Daniel Wilson. Evolutionary perspectives on human behavior during the coronavirus pandemic: insights from game theory. *Evolution, medicine, and public health*, 2020(1):181–186, 2020.
- [3] Frederick Chen. A mathematical analysis of public avoidance behavior during epidemics using game theory. *Journal of Theoretical Biology*, 302:18–28, 2012.
- [4] Frederick Chen, Miaohua Jiang, Scott Rabidoux, and Stephen Robinson. Public avoidance and epidemics: insights from an economic model. *Journal of Theoretical Biology*, 278(1):107–119, 2011.
- [5] Eli Fenichel. Economic considerations for social distancing and behavioral based policies during an epidemic. *Journal of Health Economics*, 32(2):440–451, 2013.
- [6] Eli Fenichel, Carlos Castillo-Chavez, Graziano Coddia, Gerardo Chowell, et al. Adaptive human behavior in epidemiological models. *Proceedings of the National Academy of Sciences*, 108(15):6306–6311, 2011.
- [7] Nicola Gatti and Marcello Restelli. Equilibrium approximation in simulation-based extensive-form games. In *International Conference on Autonomous Agents and Multiagent Systems*, pages 199–206, 2011.
- [8] Mark Gersovitz. Disinhibition and immiserization in a model of SIS diseases. *Unpublished Papers, Johns Hopkins University*, 2010.
- [9] Nicolas Hoertel, Martin Blachier, Carlos Blanco, Mark Olfson, et al. A stochastic agent-based model of the SARS-CoV-2 epidemic in France. *Nature medicine*, 26(9):1417–1421, 2020.

[10] Ariful Kabir and Jun Tanimoto. Evolutionary game theory modelling to represent the behavioural dynamics of economic shutdowns and shield immunity in the COVID-19 pandemic. *Royal Society Open Science*, 7(9):201095, 2020.

[11] Stephen Lauer, Kyra Grantz, Qifang Bi, Forrest Jones, Qulu Zheng, et al. The incubation period of coronavirus disease 2019 (COVID-19) from publicly reported confirmed cases: estimation and application. *Annals of Internal Medicine*, 172(9):577–582, 2020.

[12] Atalanti Mastakouri and Bernhard Schölkopf. Causal analysis of COVID-19 spread in Germany. *Advances in Neural Information Processing Systems*, 33, 2020.

[13] Kiesha Prem, Alex Cook, and Mark Jit. Projecting social contact matrices in 152 countries using contact surveys and demographic data. *PLoS Computational Biology*, 13(9):e1005697, 2017.

[14] Zhaozhi Qian, Ahmed Alaa, and Mihaela van der Schaar. When and How to Lift the Lockdown? Global COVID-19 Scenario Analysis and Policy Assessment using Compartmental Gaussian Processes. *Advances in Neural Information Processing Systems*, 2020.

[15] Timothy Reluga. Game theory of social distancing in response to an epidemic. *PLoS Computational Biology*, 6(5):e1000793, 2010.

[16] Rick Rojas. Trump criticizes Georgia governor for decision to reopen state. *New York Times*, 2020. Accessed: 2020-01-19.

[17] Bob Rowthorn and Flavio Toxvaerd. The optimal control of infectious diseases via prevention and treatment. *CEPR Discussion Paper No. DP8925*, 2012.

[18] Robert Rowthorn and Jan Maciejowski. A cost–benefit analysis of the covid-19 disease. *Oxford Review of Economic Policy*, 36(Supplement):S38–S55, 2020.

[19] Suresh Sethi. Optimal quarantine programmes for controlling an epidemic spread. *Journal of the Operational Research Society*, pages 265–268, 1978.

[20] Mrinank Sharma, Sören Mindermann, Jan M Brauner, Gavin Leech, Anna B Stephenson, Tomáš Gavenciak, Jan Kulveit, Yee Whye Teh, Leonid Chindelevitch, and Yarin Gal. How Robust are the Estimated Effects of Nonpharmaceutical Interventions against COVID-19? *Advances in Neural Information Processing Systems*, 2020.

[21] Yoav Shoham and Kevin Leyton-Brown. *Multiagent systems: Algorithmic, game-theoretic, and logical foundations*. Cambridge University Press, 2008.

[22] Flavio Toxvaerd. Rational disinhibition and externalities in prevention. *International Economic Review*, 60(4):1737–1755, 2019.

[23] Flavio Toxvaerd. Equilibrium Social Distancing, 2020. Cambridge–INET Working Paper Series No. 2020/08.

[24] Jay Van Bavel, Katherine Baicker, Paulo Boggio, Valerio Capraro, et al. Using social and behavioural science to support COVID-19 pandemic response. *Nature Human Behaviour*, pages 1–12, 2020.

[25] Yevgeniy Vorobeychik and Michael Wellman. Stochastic search methods for Nash equilibrium approximation in simulation-based games. In *International Conference on Autonomous Agents and Multiagent Systems*, pages 1055–1062, 2008.

[26] Yevgeniy Vorobeychik, Daniel Reeves, and Michael Wellman. Constrained automated mechanism design for infinite games of incomplete information. In *Conference on Uncertainty in Artificial Intelligence*, pages 400–407, 2007.

[27] Michael Wellman. Methods for empirical game-theoretic analysis. In *AAAI Conference on Artificial Intelligence*, pages 1552–1556, 2006.

[28] Bryan Wilder, Marie Charpignon, Jackson Killian, Han-Ching Ou, Aditya Mate, Shahin Jabbari, et al. Modeling between-population variation in COVID-19 dynamics in Hubei, Lombardy, and New York City. *Proceedings of the National Academy of Sciences*, 117(41):25904–25910, 2020.

## A Omitted Details from Section 2.3

We will state and prove a useful property of Poisson distributions.

**Proposition 1.** *Consider a random variable  $Y \sim \text{POISSON}(\lambda)$ . Then, for any non-zero real number  $b$  independent of  $Z$ ,*

$$\mathbb{E}_Z[b^Z] = e^{-\lambda(1-b)}.$$

*Proof.* From definitions,

$$\begin{aligned} \mathbb{E}_Z[b^Z] &= \sum_{z=0}^{\infty} a^z \Pr[Z = z] = \sum_{z=0}^{\infty} a^z \cdot \frac{e^{-\lambda} \lambda^z}{z!} \\ &= e^{-\lambda} \sum_{z=0}^{\infty} \frac{(b\lambda)^z}{z!} = e^{-\lambda} e^{b\lambda} \end{aligned}$$

which equals the desired expression.  $\square$

## B Omitted Details from Section 3

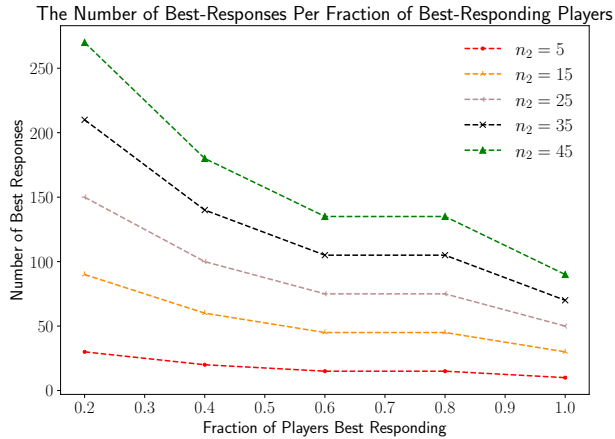


Figure 7: The number of best response steps (y-axis) as a function of the fraction of players that are best responding (x-axis). Each curve corresponds to a game with  $n_2$  players (ranging from 5 to 45) in the second level which is also the lowest level of game.

We conduct this experiment on a two-level game with one Government and a variable number  $n_2$  of States. We focus on symmetric settings, i.e. all states have equal population, equal initial infections, and equal weight vectors. The transport matrix is also symmetric. Figure 7 shows that setting  $k_2 = n_2$  in Algorithm 1 (synchronous BRD) results in fastest convergence to equilibrium for several choices of  $n_2$ .

## C Omitted Details from Section 4.1

We will first look at the variation in State 1 and 2's policies separately (Figures 8 and 9 respectively), rather than their difference, as we vary their shared non-compliance weight for the experimental set-up in Section 4.1. Recall that the initial infection rate of State 1 is fixed at 0.1 and we wish to uncover conditions under which State 2 ends up free-riding, i.e. setting a weak policy ( $\alpha_2$  close to 1) while State 1 adopts a strong policy ( $\alpha_1$  close to 0).

The most striking observation is that State 1 maintains a maximally strict policy in equilibrium for a wide range of parameters (up to a compliance weight of around 0.15 for all initial infection rates of State 2 studied here) while jumps to a fairly weak policy quickly over the same range.

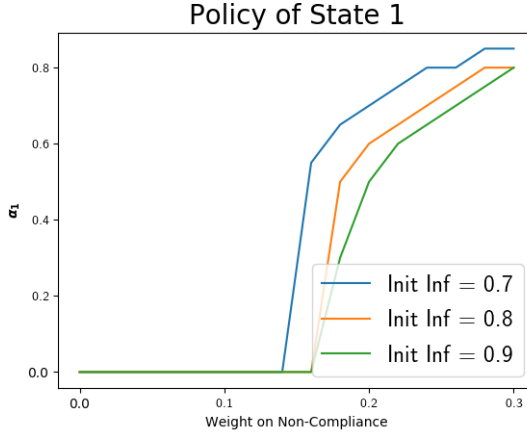


Figure 8: The Policy of State 1 (y-axis) as a function of non-compliance weight (x-axis) under transport symmetry. Each curve corresponds to a different initial infection rate for State 2 as specified in the legend.

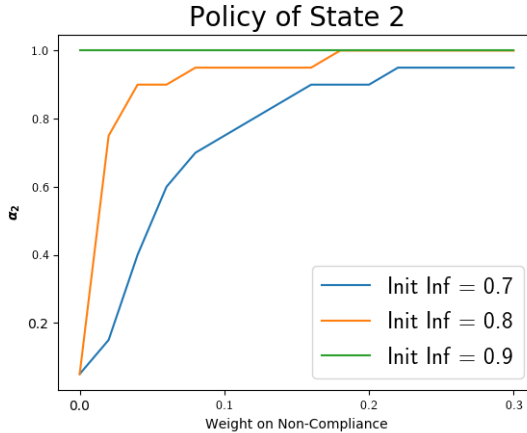


Figure 9: The Policy of State 2 (y-axis) as a function of non-compliance weight (x-axis) under transport symmetry. Each curve corresponds to a different initial infection rate for State 2 as specified in the legend.

Now turning to the setting with transport asymmetry where State 1 is the favored destination, Figures 10 and 11 provide similar insights into the behaviors of States 1 and 2 individually. Even when State 2's initial infection rate exceeds that of State 1 (which now has the moderate value 0.5), State 1 now prefers to enforce

no policy intervention for (almost) all values of its non-compliance weight while there is more variability in the equilibrium response of State 2. Further, holding that non-compliance weight fixed at 0, Figure 12

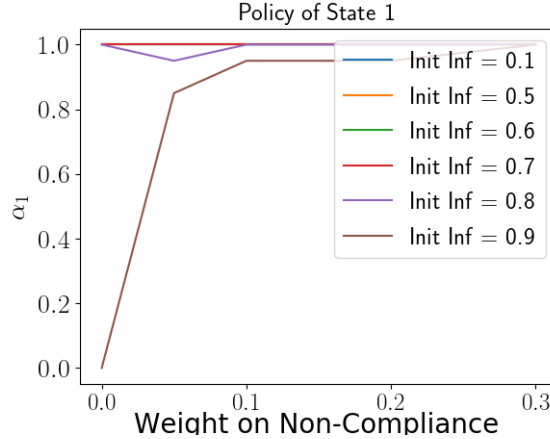


Figure 10: The Policy of State 1 (y-axis) as a function of non-compliance weight (x-axis) under our specific transport asymmetry. Each curve corresponds to a different initial infection rate for State 2 as specified in the legend.

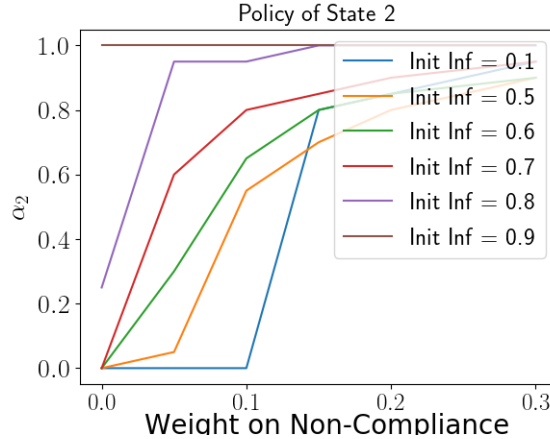


Figure 11: The Policy of State 2 (y-axis) as a function of non-compliance weight (x-axis) under our specific transport asymmetry. Each curve corresponds to a different initial infection rate for State 2 as specified in the legend.

depicts that on exceeding a threshold on its initial infection rate, State 2 chooses the weakest policy, now forcing State 1 to strengthen its own response. and causing the reversal in Figure 5.

## D Omitted Details from Section 4.2

We will first take a closer look at the policies of the Counties and the resulting Gini coefficients for the experiments in Section 4.2.

Under transport symmetry, Figures 13 give us scatter plots of the realized Gini coefficient and the equilibrium policies of all Counties for each trial respectively; Figures 15 and 16 give us the corresponding

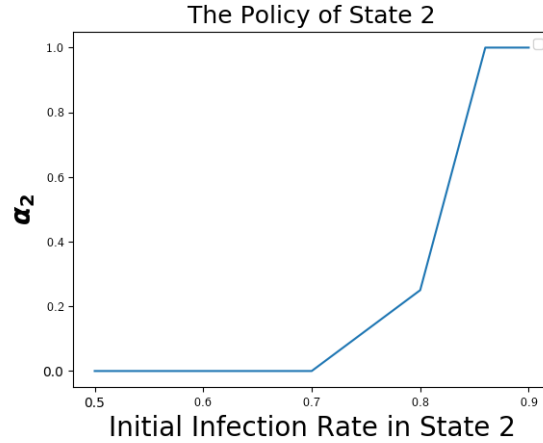


Figure 12: The Policy of State 2 (y-axis) as a function of its own initial infection rate when its weight on the non-compliance cost is 0 under our specific transport asymmetry.

scatter plots for the specific asymmetry where State 1 is the favorite destination. Important observations

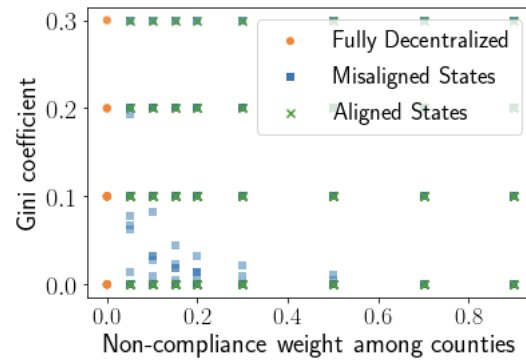


Figure 13: 50 trials for each of 3 scenarios.

on these scatter plots are that the values of the policies tend to be extreme and realized Gini coefficients seem to take on values from a small discrete set. The somewhat unique scenario is *Aligned States* which has a higher variability or granularity in values for the symmetric setting — a property that is lost under our specific asymmetry.

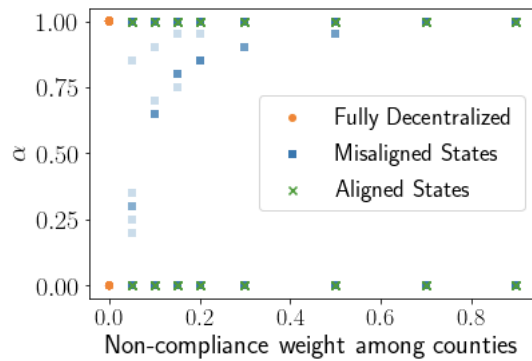


Figure 14: 50 trials for each of 3 scenarios.

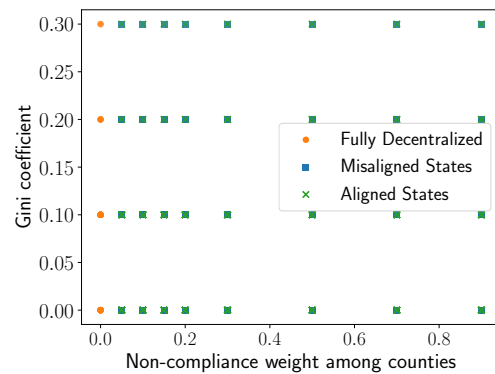


Figure 15: 30 trials for *Aligned States*, 50 trials for each other scenario.

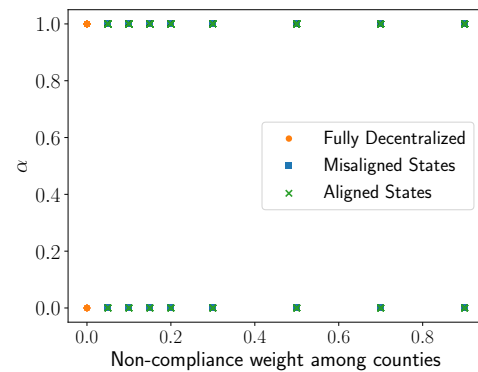


Figure 16: 30 trials for *Aligned States*, 50 trials for each other scenario.